Solid-Phase Synthesis and Insights into Structure−Activity Relationships of Safinamide Analogues as Potent and Selective Inhibitors of Type B Monoamine Oxidase

Francesco Leonetti,[§] Carmelida Capaldi,[§] Leonardo Pisani,[§] Orazio Nicolotti,[§] Giovanni Muncipinto,[§] Angela Stefanachi,[§] Saverio Cellamare,[§] Carla Caccia,[#] and Angelo Carotti*,[§]

Dipartimento Farmaco-Chimico, University of Bari, Via Orabona 4, I-70125 Bari, Italy, and Newron Pharmaceuticals, Via L. Ariosto 21, Bresso, Italy

Safinamide, (*S*)-*N*[2]-{4-[(3-fluorobenzyl)oxy]benzyl}alaninamide methanesulfonate, which is in phase III clinical trials as an anti-Parkinson drug, and a library of alkanamidic analogues were prepared through an expeditious solid-phase synthesis and evaluated for their monoamine oxidase B (MAO-B) and monoamine oxidase A (MAO-A) inhibitory activity and selectivity. (*S*)-3-Chlorobenzyloxyalaninamide (**8**) and (*S*)-3-chlorobenzyloxyserinamide (**13**) derivatives proved to be more potent MAO-B inhibitors than safinamide (IC$_{50}$ = 33 and 43 nM, respectively, vs 98 nM) but with a lower MAO-B selectivity (SI = 3455 and 1967, respectively, vs 5918). The highest MAO-B inhibitory potency (IC$_{50}$ = 17 nM) and a good selectivity (SI = 2941) were displayed by (*R*)-**21**, a tetrahydroisoquinoline analogue of safinamide. Structure−affinity relationships and docking simulations pointed out strong negative steric effects of α-aminoamide side chains and para substituents of the benzyloxy groups and favorable hydrophobic interactions of meta substituents. The significantly diverse MAO-B affinities of a number of *R* and *S* α-aminoamide enantiomers, including the two rigid analogues (**21**) of safinamide, indicated likely enantioselective interactions at the enzymatic binding sites.

Introduction

Monoamino oxidases (MAOs[a]) are flavin adenine dinucleotide (FAD) containing enzymes localized in the outer mitochondrial membrane.[1] MAOs are involved in the oxidative deamination of important endogenous amines, including monoamine neurotransmitters serotonin (5-HT), norepinephrine (NE), and dopamine (DA), as well as exogenous amines, comprising the hypertensive dietary amine tyramine.[2] Two different isoenzymatic forms have been identified, namely, MAO-A and MAO-B,[3] which differ in their amino acid sequences, three-dimensional structures,[4,5] and substrate specificity and sensitivity to inhibitors.[6] Selective MAO-B inhibitors (i.e., selegiline and rasagiline, Chart 1)[7] are used, alone or in combination with L-DOPA, in the symptomatic treatment of Parkinson's disease, whereas selective MAO-A inhibitors (i.e., moclobemide, Chart 1) are employed as antidepressants.[8−10] The important side effects associated with the use of selegiline and to a lesser extent rasagiline, likely due to their irreversible mechanism of inhibition, and the growing interest in MAO-B inhibitors as potential anti-Alzheimer's agents[11] called for new studies aimed at the discovery of novel potent, selective, and, most importantly, truly reversible MAO-B inhibitors.

Along this line of research, Newron Pharmaceuticals recently developed safinamide ((*S*)-*N*[2]-{4-[(3-fluorobenzyl)oxy]benzyl}-alaninamide methanesulfonate) (Chart 1), initially reported by Pharmacia & Upjohn as a potent anticonvulsant,[12] which has just entered phase III clinical trials in Europe as an anti-Parkinson drug.[13−15] Indeed, safinamide acts by means of multiple mechanisms of action that comprise MAO-B and dopamine uptake inhibition, sodium and calcium channel

Chart 1. Chemical Structures of Selective MAO-A (**A**) and MAO-B (**B**) Inhibitor Drugs and of Safinamide (Methanesulfonate) **7**
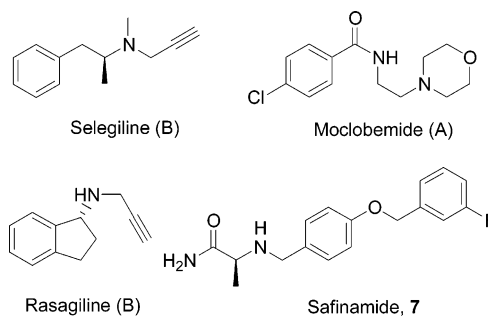
modulation, and reduction of glutamate release in the central nervous system.[16] The synthesis of safinamide has been carried out at Pharmacia & Upjohn several years ago by a conventional synthetic pathway from (*S*)-alaninamide.[12]

As part of our collaboration with Newron Pharmaceuticals and in continuation of our long-dated research in the field of MAO inhibition,[17−24] we deemed it important to develop an alternative synthetic protocol more suited for the preparation of focused libraries of safinamide congeners and aimed at an in-depth exploration of structure−affinity (SAFIR) and structure−selectivity (SSR) relationships and a further optimization of the pharmacokinetic and pharmacological properties of safinamide.

Multiple parallel syntheses, either in the solid phase or in solution, are currently used by medicinal chemists to prepare large libraries of compounds addressing specific pharmacological targets or to discover and optimize new leads.[25,26] Two different solid-phase-based approaches are actually employed: the conventional solid-phase organic synthesis (SPOS) on polymeric support[27] and the synthesis driven by polymer-supported solid reagents.[28] For the preparation of safinamide and related analogues, we chose the conventional solid-phase

Chart 2. Retrosynthetic Analysis of Safinamide **7**[a]
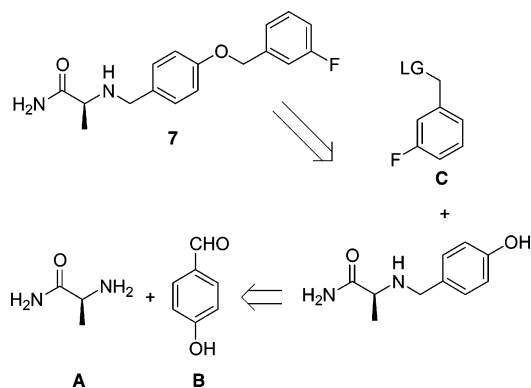
[a] LG: leaving group.

Scheme 1. Solid-Phase Synthesis of Safinamide and Analogues (Compounds **1−20** in Table 1)[a]
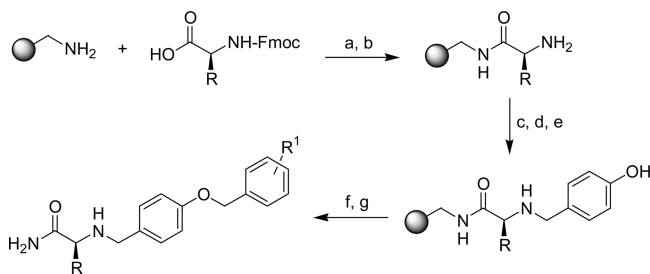
[a] Reagents and conditions: (a) HOBt, DICI, DMF, room temp, 3 h; (b) 20% piperidine in DMF, room temp, 30 min; (c) Ti(O-^{i}Pr)$_4$, TEA, THF, 4-[(triisopropylsilyl)oxy]benzaldehyde, room temp, overnight; (d) NaB-H(OCOCH$_3$)$_3$, DMC, room temp, overnight; (e) TBAF, THF, room temp, 1 h; (f) PBu$_3$, ADDP, THF, R^1-benzyl alcohol, room temp, overnight; (g) TFA/H$_2$O/TES, room temp, 1 h.

approach because it was considered to lead to cleaner reactions, easier workup, possible automation, and scalability.

Results and Discussion

Chemistry. The straightforward retrosynthetic analysis of safinamide (Chart 2) revealed three different building blocks: (*S*)-alaninamide **A**, benzaldehyde **B** and benzyl derivative **C** bearing a suitable leaving group (LG). These building blocks may be easily assembled, and more importantly, the vast commercial availability and/or simple synthetic accessibility of many of their analogues may enable the preparation of libraries endowed with large molecular diversity.

The synthetic protocol developed for the preparation of our exploratory library is outlined in Scheme 1. The choice of the initial building block to be anchored to an appropriate polymeric support was based on the observation that our target molecule is a primary amide that could be easily formed from the cleavage of a carboxylic group attached to a Rink amide resin. As the first step of our synthesis, we therefore loaded the Fmoc-(*S*)-alanine on such a resin through a conventional coupling method with HOBt and DICI in DMF. The most complex step of our synthetic pathway was the introduction of building block **B** on the support-bound amino acid. Various organic reactions could be taken into account to link building blocks **B** and **A**. We preferred reductive alkylation over nucleophilic substitution with benzyl halides or other benzyl derivatives carrying suitable LGs, since the latter might have led to a bis-alkylation of the primary amine, a highly probable side reaction in SPOS where a large excess of alkylating reagent is normally employed to drive the reaction to completion.

In our investigation the standard protocols normally used in SPOS to accomplish a reductive alkylation yielded unsatisfactory results. The use of benzaldehyde protected as the triisopropyl-silyloxy derivative (TIPS) and Ti(O-^{i}Pr)$_4$ as a Lewis acid to enhance the electrophilic character of the aldehydic carbonyl resulted in an almost quantitative yield of the aldimine intermediate. The subsequent reduction reaction was efficiently performed with a presonicated suspension of NaBH(OAc)$_3$ in DCM.[29] The ^{1}H NMR analysis of the product obtained after cleavage showed only traces of the starting amino acid, which disappeared by adding 1 equiv of triethylamine as a proton sponge during the formation of the aldimine intermediate. In the above-described experimental conditions the alkylation reaction reached completion with a very high yield.
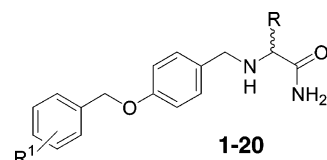
The last step of our synthetic scheme was the insertion of building block **C** that might have been accomplished through conventional benzylic nucleophilic substitutions (NSs) or more efficiently via a Mitsunobu reaction.[30] The latter was preferred because conventional NSs would have required preventive protection of the secondary amine present on the support-bound growing molecule. The Mitsunobu reaction was efficiently carried out using PBu$_3$ and ADDP. Finally, the cleavage from the resin using the TFA/H$_2$O/TES mixture afforded the target molecule in very satisfactory overall yield (nearly 60%) without any detectable trace of the starting and intermediate materials, as checked by ^{1}H NMR and HPLC analyses.

Starting from these very encouraging results we designed a small exploratory library of safinamide analogues (Table 1) to develop insightful SAFIRs and SSRs and to challenge the efficiency and versatility of our synthetic protocol. At this preliminary stage, the structural variations were limited to building blocks **A** and **C** (R and R^1 substituents in Scheme 1).

N-Fmoc-glycine, -(*S*)-alanine, -(*S*)-phenylglycine, and -(*S*)-serine were chosen as starting amino acids, and benzyl alcohol and its 3-F, 3-Cl, 4-Cl, and 4-NO$_2$ derivatives were chosen as structural variants in the Mitsunobu reaction. To our satisfaction, all 20 library compounds were obtained in overall yields and purities comparable to those observed in the synthesis of the lead compound safinamide.

Biological Assay. Rat brain mitochondria were used as the source for the two MAO isoforms. MAO enzymatic activities were assessed with a radioenzymatic assay using ^{14}C-serotonin (5-HT) and ^{14}C-phenylethylamine (PEA) as selective substrates for MAO-A and MAO-B, respectively, according to a well-consolidated procedure.[16,31] Inhibition data of both MAO isoforms were given as IC$_{50}$ (μM) or as the percentage of inhibition at the indicated concentration for low-active inhibitors. Selectivity was expressed as selectivity index (SI), which is the ratio of the IC$_{50}$ of MAO-A to the IC$_{50}$ of MAO-B. For compounds with sufficiently high aqueous solubility and high MAO-B affinity (i.e., (*S*)-**6** to (*S*)-**8** and (*S*)-**11** to (*S*)-**13**), the IC$_{50}$ at MAO-A was measured even in the case of low-active compounds to determine the SI. Chemical structures, MAO inhibition, and selectivity data of the 20 library members are reported in Table 1.

Several interesting insights emerged from the analysis of the SAFIRs and SSRs. All the synthesized compounds bound MAO-B isoform with higher affinity than MAO-A, leading to SIs ranging from 2.3 to 5918. Also, for the low-active MAO-A inhibitors, whose IC$_{50}$ was not measured, comparison of the percentages of inhibition of the two isoforms was indicative of SI values greater than 1. The highest MAO-B selectivities were shown by the meta-halogen-substituted derivatives (*S*)-**7** and (*S*)-**8** and by (*S*)-**12** and (*S*)-**13** belonging to the alanine and

**Table 1.** Inhibition Data[a] of 2[(4-Benzyloxy)benzylamino]alkanamides

compd	R	R^1	MAO-A	MAO-B	SI[c]
1[b]	H	H	8.5	3.15	2.7
2	H	3-F	13.6	2.24	6.1
3	H	3-Cl	37	0.34	109
4	H	4-Cl	12.4	7.10	1.7
5	H	4-NO$_2$	21.2	9.10	2.3
(*S*)-**6**[b]	CH$_3$	H	101	0.26	388
(*S*)-**7**	CH$_3$	3-F	580	0.098	5918
(*R*)-**7**[b]	CH$_3$	3-F	42	0.45	93
(*S*)-**8**	CH$_3$	3-Cl	114	0.033	3455
(*R*)-**8**	CH$_3$	3-Cl	72	0.80	90
(*S*)-**9**	CH$_3$	4-Cl	37%	2.20	nd[d]
(*S*)-**10**	CH$_3$	4-NO$_2$	22%	37%	nd[d]
(*S*)-**11**[b]	CH$_2$OH	H	90	0.41	220
(*S*)-**12**	CH$_2$OH	3-F	100	0.14	714
(*S*)-**13**	CH$_2$OH	3-Cl	84.6	0.043	1967
(*R*)-**13**	CH$_2$OH	3-Cl	100	0.11	909
(*S*)-**14**	CH$_2$OH	4-Cl	47%	1.10	nd[d]
(*S*)-**15**	CH$_2$OH	4-NO$_2$	38%	7.01	nd[d]
(*S*)-**16**	C$_6$H$_5$	H	35%	73.8	nd[d]
(*S*)-**17**	C$_6$H$_5$	3-F	34	10.0	3.4
(*S*)-**18**	C$_6$H$_5$	3-Cl	33%	10.1	nd[d]
(*S*)-**19**	C$_6$H$_5$	4-Cl	27%	34%	nd[d]
(*S*)-**20**	C$_6$H$_5$	4-NO$_2$	16%	4%	nd[d]
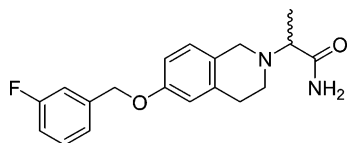
tetrahydroisoquinoline rigid analogues of **7**	MAO-A	MAO-B	SI[c]
(*S*)-**21**	45	0.24	187.5
(*R*)-**21**	50	0.017	2941

[a] Inhibition data are expressed as IC$_{50}$ (μM) or as % of inhibition at 10 μM, *r*MAO-B or 100 μM, *r*MAO-A; the SEM was always less than ±10%. [b] Described in ref 12. [c] SI = selectivity index, that is, IC$_{50}$(MAO-A)/IC$_{50}$(MAO-B). [d] nd: not determined.

serine series, respectively. Indeed, in all four series, *m*-halogenobenzyloxy derivatives showed SIs greater than the corresponding unsubstituted lead compounds. The highest SIs were observed for the 3-F- and 3-Cl-benzyloxyalaninamides (*S*)-**7** and (*S*)-**8** (SI = 5918 and 3455, respectively) and for the 3-F- and 3-Cl-benzyloxyserinamides (*S*)-**12** and (*S*)-**13** (SI = 714 and 1967, respectively). Noticeably, the introduction of halogen substituents in the meta position resulted in a significant increase of MAO-B affinity in all four amino acid series, leading in the alanine and serine series to the most potent MAO-B inhibitors of the entire series examined (i.e., the 3-chlorobenzyloxy derivatives (*S*)-**8** and (*S*)-**13** showing an IC$_{50}$ of 33 and 43 nM, respectively). Conversely, a strong drop of MAO-B affinity resulted from the introduction of a chloro and, more so, of a nitro group at the para position of the benzyloxy fragment (compare affinity of **4** and **5** vs **1**; (*S*)-**9** and (*S*)-**10** vs (*S*)-**6**; (*S*)-**14** and (*S*)-**15** vs (*S*)-**11**; (*S*)-**20** and (*S*)-**19** vs (*S*)-**16**). The notably diverse electronic and hydrophobic properties of these two para substituents may suggest a negative steric effect as the most likely cause of the observed decrease in affinity. An even stronger steric effect might be advocated to explain the dramatic fall of MAO-B affinity observed for the

Scheme 2. Synthesis of (*S*)- and (*R*)-Enantiomers of Tetrahydroisoquinoline Derivative **21**[a]
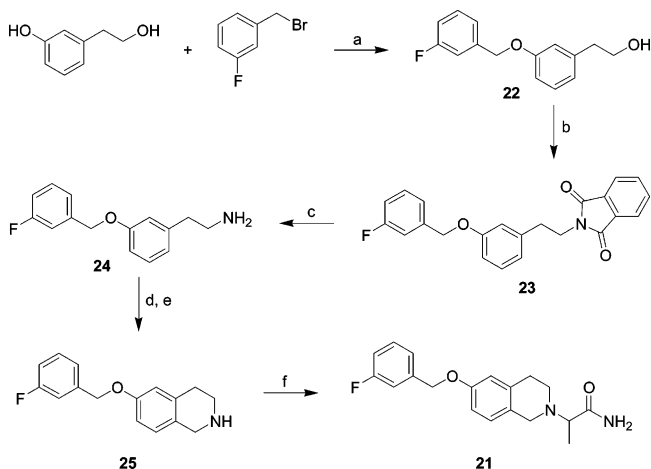
[a] Reagents and conditions: (a) K$_2$CO$_3$, KI, acetone, reflux, overnight; (b) DEAD, PS−PPh$_3$, THF, phthalimide, room temp, overnight; (c) NH$_2$NH$_2$, H$_2$O, absolute EtOH, reflux, 5 h; (d) 40% CH$_2$O, room temp, 2 h; (e) 23% HCl, room temp, 5 h; (f) (*S*)- or (*R*)-2-amino-1-methyl-2-oxoethyl-2-nitrobenzenesulfonate, DIPEA, DCM, room temp, overnight.

(*S*)-phenylglycine derivatives **16**−**20** compared to the corresponding congeners of the other three series, indicating that the amino acid side chain R strongly influenced MAO-B affinity. In fact, while comparable MAO-B inhibitory potencies were observed for the alanine and serine derivatives, significantly lower potency and selectivity emerged from the glycine series. These results suggested that favorable interactions took place at the R region irrespective of the different hydrophobic, electronic, and hydrogen-bonding properties of the methyl and hydroxymethyl groups.

To further expand the SAFIR and SSR, the (*R*)-enantiomers of three very potent and selective inhibitors (i.e., (*S*)-**7**, (*S*)-**8**, and (*S*)-**13**) were prepared along with the two enantiomers of the rigid tetrahydroisoquinoline analogue **21** (Scheme 2).

Structures, inhibition, and selectivity data of these additional MAO inhibitors are reported in Table 1.

The (*R*)-enantiomers of serinamide derivative **13** and safinamide **7** showed both lower MAO-B affinity and selectivity than the corresponding (*S*)-enantiomers: IC$_{50}$ = 0.11 μM and SI = 909 for (*R*)-**13** compared to 0.043 μM and 1967, respectively, for (*S*)-**13**; IC$_{50}$ = 0.45 μM and SI = 93 for (*R*)-**7** compared to 0.098 μM and 5918, respectively, for (*S*)-**7** (safinamide). Unexpectedly, the corresponding enantiomers of the safinamide tetrahydroisoquinoline rigid analogue **21** gave opposite inhibition results, the (*S*)-enantiomer being less active and selective than the (*R*)-enantiomer: (*S*)-**21**, IC$_{50}$ = 0.24 μM and SI = 187.5 compared to 0.017 μM and 2941, respectively, for (*R*)-**21**.

Docking Studies. To assist in the interpretation of SAFIRs and increase our understanding of the main binding interactions at MAO active sites, docking studies were performed on glicinamide derivative **2**, (*S*)-inhibitors **6**, **8**, **12**, **17**, and **20**, and both the racemic forms of safinamide **7**, serinamide derivative **13** and tetrahydroisoquinoline derivative **21** (Table 1). On the basis of a recent work conducted in our group,[23] the GOLD 3.1 program was chosen for docking simulations on the X-ray structure of rat MAO-A (*r*MAO-A, PDB code 1O5W) and on the homology model of rat MAO-B (*r*MAO-B) developed from a human MAO-B (*h*MAO-B) crystallographic structure (1OJC code in the PDB)[4] as already described.[23] Four structural water molecules, located in proximity to the FAD cofactor and labeled
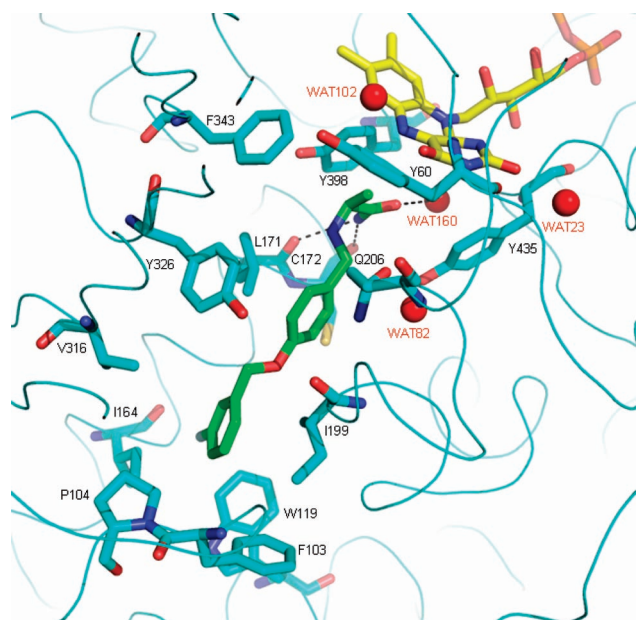
Figure 1. Docking pose of safinamide (green stick model) into *r*MAO-B. Amino acid residues of the binding site and FAD cofactor are rendered as stick models with carbon atoms in cyan and yellow, respectively, while the protein backbone is displayed as a cyan ribbon. Four structural water molecules are represented as red balls. Black dashed lines are drawn among atoms involved in HB interactions.

Figure 2. Overlaid docking poses of inhibitors **2**, (*S*)-**12**, (*R*)-**21**, and (*S*)-**21** into *r*MAO-B, rendered as colored wire models, show a binding conformation similar to that observed with safinamide (green stick model).

as WAT23, WAT82, WAT102, and WAT160 according to the numbering reported for the *h*MAO-B crystallographic structure,[4] were included in the model. The interested reader is referred to our original paper[23] for a more detailed description of the computational procedures adopted for docking simulations and water molecule location and elsewhere[32] for an in-depth discussion of principles and methods implemented in GOLD for energy calculations, conformational search, and clustering.

A preliminary docking investigation aimed at understanding how the lead compound safinamide interacted at the *r*MAO-A and -B active sites revealed a similar binding mode but with a different docking score (i.e., much higher for *r*MAO-B), in conformity with the remarkable MAO-B selectivity observed for safinamide (SI = 5918). The availability of a larger number of IC$_{50}$ values for MAO-B inhibitors prompted us to study their binding at the *r*MAO-B active site in greater detail. Docking results showed that close binding modes were largely adopted by safinamide at *r*MAO-B. In particular, it was observed that the terminal amide group, located in front of the isoalloxazine ring of FAD, acted as a molecular harpoon establishing a network of hydrogen bonds with structural WAT-160 and both the carbonyl oxygen atoms of L171 and C172 (Figure 1).

The benzyloxy molecular tail was embedded into a hydrophobic pocket delimited by F103, P104, W119, I199, V316 (I in *h*MAOB), I164 (L in *h*MAOB), and Y326, with its *m*-fluoro substituent pointing toward I164. A hierarchical cluster analysis, carried out on the entire family of conformers generated during the free docking run, revealed that all the docking poses could be collected in one prevalent geometric group within an rms value of 3.27 Å, the fitness score for the more stable docking pose being equal to 64.90 kJ/mol. Starting with the results of the above simulations, a number of additional docking runs were executed to evaluate the impact of the different R^1 and R substituents on the inhibitory potency. The top docking pose of safinamide (Figure 1) was taken as a reference to guide the binding modes of all of the other safinamide analogues. To this end, some physical constraints were set to improve the local
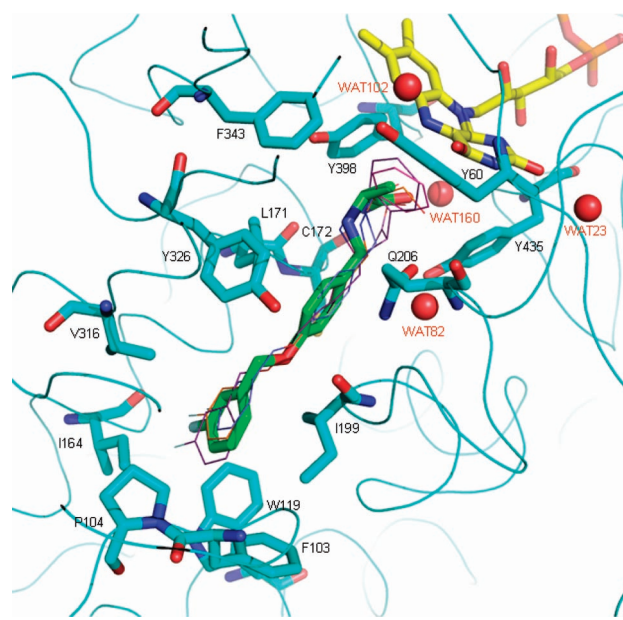
search of ligand−target interactions within the enzyme binding site (see Experimental Section).

By use of this approach, the best docking poses for safinamide derivatives were chosen not only on the basis of score energy but also on the minimum rms value resulting from their superposition onto the safinamide top-scored molecular pose. Considering all the docking poses having the least rms deviation in the safinamide binding model (Figure 2), the different R side chains of the 3-F-benzyloxy derivatives yielded the following score ranking that was consistent with the inhibitory data reported in Table 1: (*S*)-**7** (R = CH$_3$, IC$_{50}$ = 0.098 μM, score = 64.99 kJ/mol, rms = 0.33 Å) > (*S*)-**12** (R = CH$_2$OH, IC$_{50}$ = 0.14 μM, score = 61.01 kJ/mol, rms = 0.36 Å) > **2** (R = H, IC$_{50}$ = 3.30 μM, score = 58.01 kJ/mol, rms = 1.56 Å) > (*S*)-**17** (R = Ph, IC$_{50}$ = 10.0 μM, score = 54.87 kJ/mol, rms = 0.42 Å).

Figure 3 illustrates that the very low affinity of phenylglycine inhibitor (*S*)-**17** might be derived from unfavorable steric interactions of its phenyl ring with Y60 and a carbonyl group of FAD. The large increase of MAO-B affinity arising from the introduction of a halogen atom, especially chloro, in the meta position in the benzyloxy group was well accounted for by the docking results. Taking into account the (*S*)-alanine inhibitors, docking analyses awarded *m*-halogen derivatives with about 10 kJ/mol, as shown by the following data: (*S*)-**8** (R^1 = 3-Cl, IC$_{50}$ = 0.033 μM, score = 65.10 kJ/mol, rms = 0.80 Å) ≥ (*S*)-**7** (R^1 = 3-F, IC$_{50}$ = 0.098 μM, score = 64.99 kJ/mol, rms = 0.33 Å) ≫ (*S*)-**6** (R^1 = H, IC$_{50}$ = 0.26 μM, score = 56.14 kJ/mol, rms = 0.76 Å), whereas the *m*-chloro derivatives showed both higher potencies and docking scores (data not shown). Similar considerations hold within the series of serinamide inhibitors (data not shown).

Irrespective of the type of R substituents, a detrimental effect on inhibition was observed when a para substituent was introduced into the benzyloxy group. This unfavorable effect was more pronounced for the larger sized nitro group compared to the chloro substituent. These findings were supported by the docking simulations of the *p*-nitro derivatives that afforded lower scores compared to the corresponding unsubstituted lead
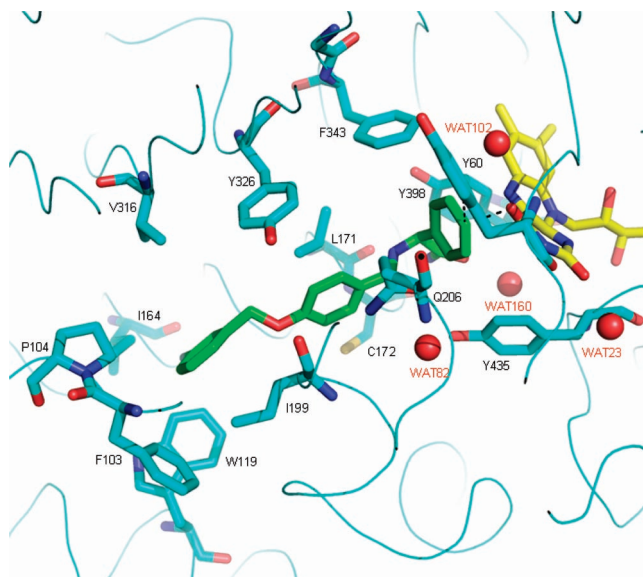
Figure 3. Docking pose of inhibitor (*S*)-**17** (displayed as a green stick model) into *r*MAO-B. Black dashed lines indicate unfavorable steric interactions among ligand phenyl side chain with FAD carbonyl oxygen and side chain of Y60.
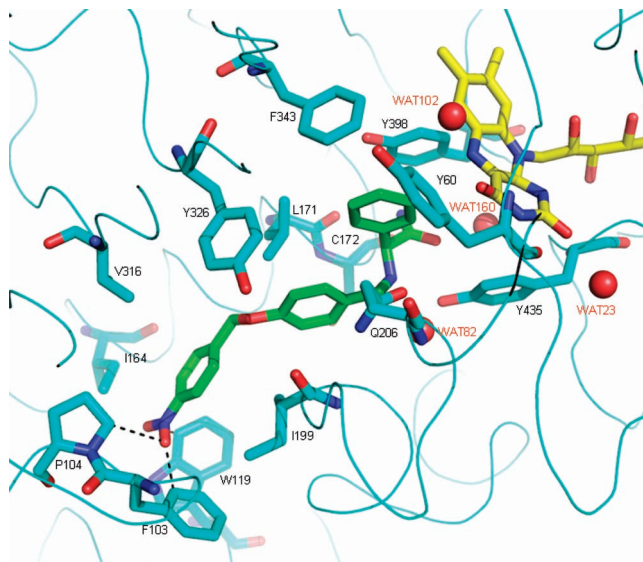

Figure 4. Docking pose of inhibitor (*S*)-**20** (displayed as a green stick model) into *r*MAO-B. Black dashed lines indicate unfavorable steric interactions among the ligand nitro group with side chains of P104, F103, and W119.

compounds. The docking pose of the lowest active *p*-nitro derivative (*S*)-**20** (Figure 4) suggested unfavorable steric interactions of the nitro group with amino acid side chains of F103, P104, and W119. Similar steric hindrance was not observed for the equally substituted 7-benzyloxycoumarin derivative,[19] and this may suggest that the anchoring benzyloxy group binds in a slightly different way in the two classes of inhibitors.

The small but significant decrease of MAO-B affinity observed moving from the (*S*)- to the (*R*)-configuration was investigated by docking the two enantiomers of the *m*-chloro-(*S*)-serine derivative **13** and safinamide **7**. In both cases scoring values consistent with a decreased inhibitory potency were found: 66.85 kJ/mol versus 60.42 kJ/mol for the (*S*)- and (*R*)-enantiomers of **13**, respectively, and 64.99 kJ/mol versus 63.52 kJ/mol for the (*S*)- and (*R*)-enantiomers of safinamide.

Finally, our docking analyses permitted proper interpretation of the unexpectedly inverted affinities of rigid tetrahydroiso-
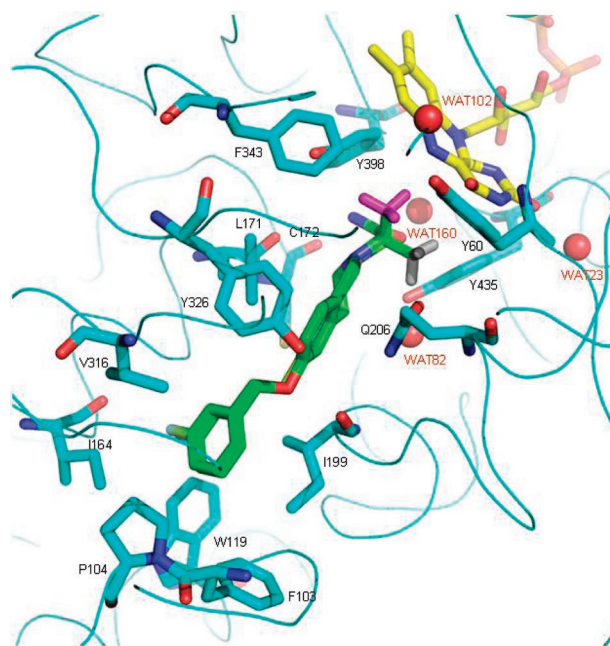

Figure 5. Overlapped docking pose of the tetrahydroisoquinoline enantiomers (*S*)-**21** and (*R*)-**21**. Energetically different hydrophobic interactions are engaged by the two methyl groups, represented in magenta and gray for the (*R*)- and (*S*)-enantiomers, respectively, with the surrounding hydrophobic side chains of Y398, Y60, and Y 435.

quinoline enantiomers **21** compared to the corresponding safinamide enantiomers. The close binding modes derived from docking simulations of the two enantiomers of **21** (Figure 5) were characterized by significantly different score values (i.e., 59.14 and 52.59 kJ/mol for (*R*)- and (*S*)-enantiomers, respectively), which are consistent with the inhibition data. The different binding energies primarily originated from a more favorable hydrophobic interaction engaged by the methyl group of the (*R*)-**21** enantiomer (shown in magenta in Figure 5) compared to the methyl group of the (*S*)-**21** enantiomer (shown in gray in Figure 5) with the surrounding hydrophobic side chains of Y398, Y60, and Y435. The methyl group of safinamide (see Figure 1) and that of its (*R*)-enantiomer were slightly displaced compared to the corresponding methyl groups of **21**, and as a consequence, they experienced similar contacts with the tyrosine side chains just mentioned.

Conclusions

Herein, we reported the SPOS of safinamide and of a small library of its analogues which were evaluated as MAO inhibitors. The proposed solid-phase synthetic protocol enabled the facile, expeditious, and high-yield preparation of a series of potent, reversible, and selective MAO B inhibitors and paved the way for the synthesis of larger libraries endowed with higher structural diversity for an in-depth exploration of SAFIRs and SSRs. Unlike the coumarin series, safinamide analogues presented excellent pharmacokinetic properties, such as higher water solubility and bioavailability, that may anticipate, as it was indeed found for safinamide, a high in vivo activity and outstanding therapeutic and toxic profiles. In the present study, α-aminoalkanamide analogues of safinamide were designed to explore mostly the substituent effects at the meta and para positions of the benzyloxy group and to detect the main interactions engaged by the α-aminoamide side chain. Our findings indicated that MAO-B affinity and selectivity can be efficiently modulated by appropriate substitutions on the benzyloxy ring. In particular, as already observed in the coumarin

series, lipophilic meta substituents significantly increased both MAO-B affinity and selectivity. Large and rigid α-aminoamide side chains were not tolerated, most likely for steric reasons. The highest inhibitory potencies were observed for the 3-chlorobenzyloxyalanine and 3-chlorobenzyloxyserine derivatives (*S*)-**8** and (*S*)-**13**, respectively, and by the (*R*)-3-F-benzyloxytetrahydroisoquinoline derivative **21**, which displayed the highest affinity of the entire series of examined inhibitors (IC$_{50}$ = 17 nM) along with an outstanding selectivity (SI = 2941).

Docking studies enabled the identification of the physicochemical nature and spatial location of the main binding interactions modulating the enzymatic affinity and selectivity of safinamide analogues. The high MAO-B selectivity of safinamide was nicely interpreted by docking simulations which yielded a much higher score for *r*MAO-B than *r*MAO-A. Furthermore, docking poses of all the inhibitors disclosed favorable interactions of the benzyloxy group, which took place in the entrance cavity of the MAO-B binding site, whereas α-aminoamide groups bind in the FAD region establishing HB interactions with structured water molecules and polar groups of the enzyme backbone. In conclusion, the present study reinforced and complemented, especially in the less explored FAD region, the interaction models proposed by our group for selective MAO-B inhibition[19,20,23] and deepened our understanding of the structural requirements for high MAO-B affinity and selectivity. The ease of synthetic accessibility and fine druglike properties of safinamide analogues make them "privileged molecules" for further structural modifications in the preparation of novel and improved neuroprotective agents. However, particular care has to be taken in the design of new *h*MAO-B inhibitors because SAFIR and SSR might vary among species.[21,24]

Experimental Section

Chemistry. Starting materials, reagents, and solvents of high analytical grade were purchased from commercial suppliers. The Rink amide resin, loading level of 0.64 mmol/g, was from Novabiochem. Chromatographic separations were performed on silica gel (15−40 mesh, Merck) by the flash methodology unless otherwise stated. Tetrahydrofuran (THF) and dichloromethane (DCM) were made anhydrous by reflux on sodium/benzophenone ketyl and calcium hydride, respectively, and distillation under N$_2$. Melting points were determined by the open capillary method on a Stuart-Scientific SMP3 electrothermal apparatus and are uncorrected. ^{1}H NMR spectra were recorded in the indicated deuterated solvents at 300 MHz on a Varian Mercury 300 instrument. Chemical shifts are expressed in δ (ppm) and coupling constants *J* in hertz (Hz). The following abbreviations were used for multiplicities: br (broad), s (singlet), d (doublet), t (triplet), dd (double doublet), dt (double triplet), ddd (double doublet of doublet), q (quintet), m (multiplet); signals due to OH protons were located by deuterium exchange with D$_2$O. Elemental analyses (C, H, N) were performed only for the *S* and *R* chiral enantiomers of tetrahydroisoquinoline derivative **21**, prepared through conventional solution-phase synthesis, whereas for all the compounds synthesized by SPOS and for the intermediates **22−26** as well, the purity was checked by ^{1}H NMR and HPLC. All the tested compounds had a purity of >95%. HPLC analyses were carried out on a Waters 1585 system equipped with a model 2487 UV detector, a Waters XTerra C8 column (3 mm × 250 mm), and different MeOH/H$_2$O mixtures as the mobile phase. Chiral HPLC analyses were run on a CHIRALPAK IA (4.6 mm × 250 mm) column (Daicel Chemical Industries, Japan) or a CHIROBIOTIC TAG (4.6 mm × 250 mm) column (Astec Separation Technologies Inc.). Mobile phases used on the CHIRALPAK column were made of 20−30% of ethanol in hexane, while 60−65% of MeOH in water was used as the mobile phase on the CHIROBIOTIC TAG column (see Table 1 in the Supporting Information for additional details). The enantiomeric excess

measured for all the chiral compounds listed in Table 1 was always >98%. ^{1}H NMR spectral data of compounds **1−20** were reported in the Supporting Information.

Synthesis. General Procedure for SPOS of Safinamide 7 and Analogues (1−6 and 8−20). An amount of 125 mg (0.08 mmol) of Rink amide resin was placed in 20 different reactor vessels (QUEST 210 apparatus), followed by swelling with 2 mL of DMF for 0.5 h. After filtration, a 20% solution of piperidine in DMF (1.5 mL) was added to each reactor vessel, and the mixture was shaken for 30 min. The resin was then filtered and washed three times with 2 mL of DMF. To four separate 25 mL round-bottom flasks were added 2.0 mmol of the selected Fmoc-protected amino acid (Gly, Ser, Ala, Phg), HOBt (2.0 mmol, 0.30 g), DICI (2.0 mmol, 0.31 mL), and DMF (10.0 mL). After the mixture was stirred for 3 min at room temperature, each solution was divided into five 2 mL aliquots and 0.50 mL of each of them was added to the 20 reactor vessels followed by shaking for 3 h. A bromophenol test was employed to monitor the reaction completion. The resin was filtered and washed three times with 2 mL of DMF. After Fmoc deprotection with piperidine in DMF and washing, the amino terminus was alkylated by adding to each vessel *p*-triisopropylsilyloxybenzaldehyde (0.40 mmol, 0.12 g), Ti(O-^{i}Pr)$_4$ (0.55 mmol, 0.15 g), and TEA (0.08 mmol, 11.1 μL). After the mixture was stirred at room temperature overnight, the resin was filtered and washed with anhydrous THF (3 × 2 mL) and anhydrous DCM (3 × 2 mL). A presonicated suspension of NaBH(OAc)$_3$ (0.40 mmol, 0.09 g) in DCM (1.5 mL) was added to the resin. The mixture was stirred on an orbital shaker overnight, then filtered and washed in sequence with water (3 × 2 mL), 0.75 M Na$_2$CO$_3$ aqueous solution (3 × 2 mL), water (3 × 2 mL), THF (3 × 2 mL), and MeOH (3 × 2 mL) and dried under N$_2$ flow. THF (1.5 mL) was added to each vessel, and the slurries were shaken for 30 min, filtered, treated with 1 M solution of TBAF in THF (1.5 mL) for 1 h, and then filtered again and washed with THF (3 × 2 mL). Finally, the phenolic hydroxyl group was alkylated by the Mitsunobu protocol using five different benzyl alcohol derivatives (see Table 1) as follows: 1.3 mL of a 0.2 M solution of the appropriate benzyl alcohol in DMF was added to the appropriate support-bound 2-(*p*-hydroxybenzyl)-2-aminoamide (see Scheme 1) in order to have the final 20-member library (5 benzyl alcohols × 4 aminoamides). To each reaction vessel were subsequently added PBu$_3$ (0.24 mmol, 0.06 mL) and ADDP (0.24mmol, 0.06 g), and the slurries were shaken overnight. The mixtures were filtered off, the resins washed with THF (3 × 2 mL), DMF (3 × 2 mL), THF (3 × 2 mL), MeOH (3 × 2 mL), and DCM (3 × 2 mL) and then treated for 1 h with 2 mL of a TFA/H$_2$O/TES (95/2.5/2.5) mixture. The mixture was filtered and the resin washed with the same mixture of cleavage (3 × 2 mL). The filtrate and washing solvent mixtures were combined and immediately concentrated with evaporation under reduced pressure. Toluene (2 × 2 mL) was added during the concentration step in order to remove the remaining TFA. The compounds were isolated as free bases, generally with a purity of >90%. When necessary, the crude compound was purified by flash chromatography using a mixture of DCM/MeOH as eluent.

^{1}H NMR spectral data of compounds **1−20** are described in the Supporting Information.

2-[3-(3-Fluorobenzyloxy)phenyl]ethanol (22). 3-(2-Hydroxyethyl)phenol (7.2 g, 51.9 mmol), 3-fluorobenzyl bromide (8.9 g, 47.2 mmol), K$_2$CO$_3$ (19.6 g, 141.5 mmol), and KI (1.0 g, 6.1 mmol) in acetone (65 mL) were refluxed under mechanical stirring overnight. The reaction mixture was filtered to remove inorganic salts and evaporated under vacuum to dryness. The crude residue was dissolved in EtOAc, washed with 0.5 N NaOH and brine, dried over Na$_2$SO$_4$, filtered, and evaporated to dryness. An amount of 11.8 g of the desired compound (100% yield) was obtained as a yellow oil. This crude material was utilized in the following reaction without further purification. ^{1}H NMR (CDCl$_3$) δ 2.85 (t, 2H, *J* = 7.5), 3.85 (t, 2H, *J* = 7.5), 5.06 (s, 2H), 6.79−6.91 (m, 3H), 6.96−7.06 (m, 1H), 7.11−7.28 (m, 3H), 7.29−7.40 (m, 1H).

2-{2-[3-(3-Fluorobenzyloxy)phenyl]ethyl}isoindole-1,3-dione (23). 2-[3-(3-Fluorobenzyloxy)phenyl]ethanol (8.8 g, 35.7

mmol), phthalimide (7.4 g, 50.0 mmol), triphenylphosphine polymer bound (7.4 g, 50.0 mmol, loading of 1 mmol/g), and diethyl azadicarboxylate (DEAD, 8.7 g, 50.0 mmol) were suspended in THF (320 mL) and stirred at room temperature overnight. Additional DEAD (2.7 g, 15.3 mmol) was added under stirring to the reaction mixture over a period of 5 h. The reaction mixture was filtered off, and the filtrate was evaporated to dryness. The crude residue was dissolved in EtOAc, washed with 1 N KOH and brine, dried over Na_2SO_4, filtered, and evaporated to dryness. The residue was triturated with EtOH, filtered, and then crystallized with EtOH to give 5.8 g of title compound (43% yield) as white crystals of sufficient purity for the subsequent reaction. ^{1}H NMR (CDCl₃) δ 2.93–3.03 (m, 2H), 3.90–3.99 (m, 2H), 5.02 (s, 2H), 6.82 (ddd, 1H, J = 8.3, 2.8, 1.1), 6.86–6.93 (m, 2H), 6.96–7.05 (m, 1H), 7.10–7.25 (m, 3H), 7.30–7.39 (m, 1H), 7.67–7.75 (m, 2H), 7.81–7.88 (m, 2H).

2-[3-(3-Fluorobenzyloxy)phenyl]ethylamine (24). 2-{2-[3-(3-Fluorobenzyloxy)phenyl]ethyl}isoindole-1,3-dione (2.0 g, 5.3 mmol) and hydrazine hydrate (0.58 g, 11.7 mmol) were dissolved in absolute EtOH (45 mL) under mechanical stirring and refluxed for 5 h. The formed white precipitate was filtered off, and the ethanolic filtrate was evaporated to dryness, dissolved in DCM, and washed with water. The organic layer was dried over Na_2SO_4, filtered, and evaporated to dryness to yield 1.1 g (82% yield) of the title compound as a yellow oil. This crude material was utilized in the following reaction without further purification. ^{1}H NMR (CDCl₃) δ 2.73 (t, 2H, J = 7.6), 2.97 (t, 2H, J = 7.6), 5.06 (s, 2H), 6.74–6.87 (m, 3H), 7.01 (m, 1H), 7.12–7.25 (m, 3H), 7.29–7.41 (m, 1H).

6-(3-Fluorobenzyloxy)-1,2,3,4-tetrahydroisoquinoline (25). 2-[3-(3-Fluorobenzyloxy)phenyl]ethylamine (1.5 g, 6.0 mmol), formaldehyde 40% solution in water (0.54 mL, 7.8 mmol), and water (0.54 mL) were stirred at room temperature for 2 h. The reaction mixture was evaporated to dryness, and an amount of 1.76 mL of 23% aqueous HCl was added. The mixture was stirred at room temperature for 5 h. After dilution with some water, 0.5 N aqueous NaOH was added with cooling up to pH 10. The mixture was extracted with EtOAc, washed with H_2O, dried over Na_2SO_4, filtered, and evaporated to dryness to yield 1.4 g (93% yield) of the title compound as a yellow oil. This crude material was utilized in the subsequent reaction without further purification. ^{1}H NMR (CDCl₃) δ 2.77 (t, 2H, J = 6.0), 3.11 (t, 2H, J = 6.0), 3.95 (s, 2H), 5.03 (s, 2H), 6.69 (d, 1H, J = 2.7), 6.76 (dd, 1H, J = 8.4, 2.7), 6.92 (d, 1H, J = 8.4), 6.95–7.06 (m, 1H), 7.09–7.23 (m, 2H), 7.28–7.41 (m, 1H).

(*S*)- or (*R*)-2-Amino-1-methyl-2-oxoethyl-2-nitrobenzenesulfonate. The (*S*)- or (*R*)-2-hydroxypropionamide (3.4 g, 38.0 mmol), triethylamine (7.7 g, 76.0 mmol), and *N,N*-dimethylaminopyridine (1.2 g, 9.5 mmol) were dissolved in 110 mL of DCM and cooled to 0 °C. *o*-Nitrobenzenesulfonyl chloride (16.8 g, 76.0 mmol) was added portionwise, and the mixture was stirred at room temperature overnight. The mixture was washed with water and a 10% aqueous solution of citric acid, dried over Na_2SO_4, filtered, and evaporated to dryness to yield 6.7 g of a brown oil. This crude material was purified by flash column chromatography, using 95:5 DCM/MeOH as eluent, to yield the title (*R*)- or (*S*)-enantiomer as a pale-yellow solid in a 20–25% yield and an enantiomeric excess of >98%. ^{1}H NMR (DMSO-*d₆*) δ 1.46 (d, J = 6.9, 3H), 3.28–3.61 (br, 2H), 4.45 (q, J = 6.9, 1H), 7.80–7.86 (m, 2H), 7.88–7.94 (m, 1H), 8.11–8.14 (m, 1H).

(*R*)-2-[6-(3-Fluorobenzyloxy)-3,4-dihydro-1*H*-isoquinolin-2-yl]propionamide (21). 6-(3-Fluorobenzyloxy)-1,2,3,4-tetrahydroisoquinoline (0.23 g, 0.91 mmol) dissolved in DCM (1 mL) was added dropwise at 0 °C to a solution of (*S*)-2-amino-1-methyl-2-oxoethyl-2-nitrobenzenesulfonate (0.5 g, 1.8 mmol) and DIPEA (0.24 g, 1.8 mmol) in DCM (15 mL). The reaction mixture was stirred at room temperature overnight and extracted with a 5% aqueous solution of citric acid. The aqueous layer was washed with Et₂O, made basic with 28% NH₄OH, and extracted with DCM. The organic layer was dried over Na_2SO_4, filtered, and evaporated to dryness to yield 0.14 g of title compound as a white crude solid. This crude material

was purified by a slow column chromatography, using 99:1 DCM/MeOH as eluent, to yield 0.068 g (23% yield) of a pure white solid. Mp 153–154 °C. ^{1}H NMR (CDCl₃) δ 1.35 (d, 3H, J = 7.0), 2.67–2.97 (m, 4H), 3.28 (q, 1H, J = 7.0), 3.64 (d, 1H, J = 14.2), 3.77 (d, 1H, J = 14.2), 5.05 (s, 2H), 5.36 (br, 1H), 6.74 (d, 1H, J = 2.5), 6.79 (dd, 1H, J = 8.2, 2.5), 6.97 (d, 1H, J = 8.2), 7.00–7.06 (m, 1H), 7.06–7.24 (m, 3H), 7.29–7.42 (m, 1H).

(*S*)-2-[6-(3-Fluorobenzyloxy)-3,4-dihydro-1*H*-isoquinolin-2-yl]propionamide (21). The title compound was obtained using the same procedure described for the synthesis of (*R*)-2-[6-(3-fluorobenzyloxy)-3,4-dihydro-1*H*-isoquinolin-2-yl]propionamide, starting from 6-(3-fluorobenzyloxy)-1,2,3,4-tetrahydroisoquinoline (0.24 g, 0.95 mmol) and (*R*)-2-amino-1-methyl-2-oxoethyl-2-nitrobenzenesulfonate (0.52 g, 1.9 mmol). After column chromatography purification using 99:1 DCM/MeOH as eluent, 0.075 g (24% yield) of the title compound was obtained as a pure white solid. Mp 153–154 °C. ^{1}H NMR (CDCl₃) δ 1.35 (d, 3H, J = 7.0), 2.67–2.97 (m, 4H), 3.28 (q, 1H, J = 7.0), 3.64 (d, 1H, J = 14.2), 3.77 (d, 1H, J = 14.2), 5.05 (s, 2H), 5.36 (br, 1H), 6.74 (d, 1H, J = 2.5), 6.79 (dd, 1H, J = 8.5, 2.5), 6.97 (d, 1H, J = 8.5), 6.99–7.06 (m, 1H), 7.06–7.24 (m, 3H), 7.30–7.40 (m, 1H).

Biological Assay. In Vitro Enzyme Activity Assay. The enzyme activities were assessed with a radioenzymatic assay using the selective substrates ^{14}C-serotonin (5-HT) and ^{14}C-phenylethylamine (PEA) for MAO-A and MAO-B, respectively.

The mitochondrial pellet (500 μg protein) was resuspended in 200 μL of 0.1 M phosphate buffer, pH 7.40, and was added to 50 μL of the solution of the inhibitor (transformed to the methanesulfonate salt upon addition of a stoichiometric amount of 0.01 M methanesulfonic acid to the aqueous solution of the free base) or of buffer and incubated for 30 min at 37 °C (preincubation). Then the substrate in 50 μL of buffer (5 μM ^{14}C-5-HT or 0.5 μM ^{14}C-PEA) was added and the assay mixture was incubated at 37 °C for 30 min (5-HT) or for 10 min (PEA).

The reaction was stopped by adding 0.2 mL of HCl or perchloric acid for 5-HT or PEA, respectively. After centrifugation, the acidic radioactive metabolites were extracted with 3 mL of diethyl ether (for 5-HT) or toluene (for PEA) and the radioactivity of the organic phase was measured by liquid scintillation spectrometry at 90% efficiency.

The enzymatic activity was expressed as nanomoles of substrate transformed per milligram of protein per minute (nmol mg^{-1} min^{-1}).

The drug inhibition curves were obtained from five to eight different concentrations (10^{-10}–10^{-5} M), each in duplicate, and the IC_{50} was determined using nonlinear regression analysis (GraphPad best-fitting computer program). For very low active inhibitors, the percent of enzyme inhibition was determined in duplicate at the concentrations indicated in Table.1.

Computational Methods. Computational analyses were conducted on a 16-node Linux cluster employing an openMosix architecture composed of AMD Athlon XP 2400+ and Intel Xeon 2600 cpu$_s$. Molecules and models were displayed and manipulated on a Silicon Graphics O2+ machine.

Docking Simulations. GOLD, a genetic algorithm-based software, was used for our docking study selecting the GOLDScore as a fitness function. GOLDScore is made up of four components that account for protein–ligand binding energy: protein–ligand hydrogen bond energy (external H-bond), protein–ligand van der Waals energy (external vdw), ligand internal van der Waals energy (internal vdw), and ligand torsional strain energy (internal torsion). Empirical parameters used in the fitness function (hydrogen bond energies, atom radii and polarizabilities, torsion potentials, hydrogen bond directionalities, and so forth) are taken from the GOLD parameter file. The fitness score is taken as the negative of the sum of the energy terms so that larger fitness scores indicated a better binding. The fitness function has been optimized for the prediction of ligand binding positions rather than the prediction of binding affinities, although some correlation with the latter can be also found. The protein input file may be the entire protein structure or a part of it comprising only the residues that are in the region of the ligand binding site. In the present study, GOLD was allowed

to calculate interaction energies within a sphere of a 12 Å radius centered on the phenolic oxygen atom of Y435 of *r*MAO-B and in the corresponding Y444 of *r*MAO-A. When it was explicitly specified, considering safinamide as a molecular reference, physical distance constraints were defined between the fluorine atom with the carbonyl oxygen of I164, the nitrogen of the amide group with the carbonyl oxygen atoms of C172 and L171, and, finally, the oxygen of the amide group with WAT160, the spring constant being set to 30 kJ mol^{-1} Å^{-1} and the deviation tolerance to ±0.3 Å.

Supporting Information Available: ^{1}H NMR data of compounds **1**–**20**, elemental analyses (C, H, N) of the target compound **21**, and table of chromatographic data for the assessment of enantiomeric excess. This material is available free of charge via the Internet at http://pubs.acs.org.

References

(1) Tipton, K. F. Enzymology of Monoamine Oxidase. *Cell Biochem. Funct.* **1986**, *4*, 79–87.

(2) Yamada, M.; Yasuhara, H. Clinical Pharmacology of MAO Inhibitors: Safety and Future. *Neurotoxicology* **2004**, *25*, 215–221.

(3) Johnston, J. P. Some Observation upon a New Inhibitor of Monoamine Oxidase in Brain Tissue. *Biochem. Pharmacol.* **1968**, *17*, 1285–1297.

(4) (a) Binda, C.; Newton-Vinson, P.; Hubalek, F.; Edmondson, D. E.; Mattevi, A. Structure of Human Monoamine Oxidase B, a Drug Target for a Treatment of Neurological Disorders. *Nat. Struct. Biol.* **2002**, *9*, 22–26. (b) Binda, C.; Li, M.; Hubalek, F.; Restelli, N.; Edmonson, D. E.; Mattevi, A. Insights into the Mode of Inhibition of Human Mitochondrial Monoamine Oxidase B from High-Resolution Crystal Structures. *Proc. Natl. Acad. Sci. U.S.A.* **2003**, *100*, 9750–9755.

(5) Ma, J.; Yoshimura, M.; Yamashita, E.; Nakagawa, A.; Ito, A.; Tsukihara, T. Structure of Rat Monoamine Oxidase A and Its Specific Recognitions for Substrates and Inhibitors. *J. Mol. Biol.* **2004**, *338*, 103–114.

(6) Grimsby, J.; lan, N. C.; Neve, R.; Chen, K.; Shih, J. C. Tissue Distribution of Human Monoamine Oxidase-A and Oxidase-B Messenger-RNA. *J. Neurochem.* **1990**, *55*, 1166–1169.

(7) Youdim, M. B.; Riederer, P. F. A Review of Mechanisms and Role of Monoamine Oxidase Inhibitors in Parkinson's Disease. *Neurology* **2004**, *63* (Suppl. 2), S32.

(8) Fowler, C. J.; Ross, S. B. Selective Inhibitors of Monoamine Oxidase A and B: Biochemical, Pharmacological and Clinical Properties. *Med. Res. Rev.* **1984**, *4*, 323–358.

(9) Kyburz, E. New Developments in the Field of MAO Inhibitors. *Drug News Perspect.* **1990**, *3*, 592–599.

(10) Drukarch, B.; van Muiswinkel, F. L. Drug Treatment of Parkinson's Disease. Time for Phase II. *Biochem. Pharmacol.* **2000**, *59*, 1023–1031.

(11) Riederer, P.; Danielczyk, W.; Grunblatt, E. Monoamine Oxidase-B Inhibition in Alzheimer's Disease. *Neurotoxicology* **2004**, *25*, 271–277.

(12) Pevarello, P.; Bonsignori, A.; Dostert, P.; Heidempergher, F.; Pinciroli, V.; Colombo, M.; McArthur, R. A.; Salvati, P.; Post, C.; Fariello, R. G.; Varasi, M. Synthesis and Anticonvulsant Activity of a New Class of 2-[(Arylalky)amino]alkanamide Derivatives. *J. Med. Chem.* **1998**, *41*, 579–590.

(13) Stocchi, F.; Arnold, G.; Onofrj, M.; Kwiecinski, H.; Szczudlik, A.; Thomas, A.; Bonuccelli, U.; Van Dijk, A.; Cattaneo, C.; Sala, P.; Fariello, R. G. Improvement of Motor Function in Early Parkinson Disease by Safinamide. *Neurology* **2004**, *63*, 746–748.

(14) Marzo, A.; Dal Bo, L.; Ceppi Monti, N.; Crivelli, F.; Ismaili, S.; Caccia, C.; Cattaneo, C.; Fardello, R. G. Pharmacokinetics and Pharmacodynamics of Safinamide, a Neuroprotectant with Antiparkinsonian and Anticonvulsant Activity. *Pharmacol. Res.* **2004**, *50*, 77–85.

(15) Chazot, P. L. Safinamide (Newron Pharmaceuticals). *Curr. Opin. Invest. Drugs* **2001**, *2*, 809–813.

(16) Caccia, C.; Maj, R.; Calabresi, M.; Maestroni, S.; Faravelli, L.; Curatolo, L.; Salvati, P.; Fariello, R. G. Safinamide: From Molecular Targets to a New Anti-Parkinson Drug. *Neurology* **2006**, *67*, S18–23.

(17) (a) Kneubühler, S.; Carta, V.; Altomare, C.; Carotti, A.; Testa, B. Synthesis and Monoamine Oxidase Inhibitors Activity of 3-Substituted 5*H*-Indeno[1,2-*c*]pyridazines. *Helv. Chim. Acta* **1993**, *76*, 1956–1963. (b) Kneubühler, S.; Thull, U.; Altomare, C.; Carta, V.; Gaillard, P.; Carrupt, P.-A.; Carotti, A.; Testa, B. Inhibition of Monoamine Oxidase-B by 5*H*-Indeno[1,2-*c*]pyridazines. Biological Activities, Quantitative Structure–Activity-Relationships (QSARs) and 3D-QSARs. *J. Med. Chem.* **1995**, *38*, 3874–3883. (c) Thull, U.; Kneubühler, S.; Gaillard, P.; Carrupt, P.-A.; Testa, B.; Altomare, C.; Carotti, A.; Jenner, P.; McNaught, K. S. P. Inhibition of Monamine Oxidase by Isoquinoline Derivatives: Qualitative and 3D-Quantitative Structure–Activity Relationships. *Biochem. Pharmacol.* **1995**, *50*, 869–877. (d) Altomare, C.; Cellamare, S.; Summo, L.; Catto, M.; Carotti, A.; Thull, U.; Carrupt, P.-A.; Testa, B.; Stöckli-Evans, H. Inhibition of Monoamine Oxidase-B by Condensed Pyridazines and Pyrimidines; Effects of Lipophilicity and Structure–Activity Relationships. *J. Med. Chem.* **1998**, *41*, 3812–2820.

(18) Carotti, A.; Carrieri, A.; Chimichi, S.; Boccalini, M.; Cosimelli, B.; Gnerre, C.; Carotti, A.; Carrupt, P.-A.; Testa, B. Natural and Synthetic Geiparvarins Are Strong and Selective MAO-B Inhibitors. Synthesis and SAR Studies. *Bioorg. Med. Chem. Lett.* **2002**, *12*, 3551–3555.

(19) Gnerre, C.; Catto, M.; Leonetti, F.; Weber, P.; Carrupt, P.-A.; Altomare, C.; Carotti, A.; Testa, B. Inhibition of Monoamine Oxidases by Functionalized Coumarin Derivatives: Biological Activities, QSARs, and 3D-QSARs. *J. Med. Chem.* **2000**, *43*, 4747–4758.

(20) Brühlmann, C.; Ooms, F.; Carrupt, P.-A.; Testa, B.; Catto, M.; Leonetti, F.; Altomare, C.; Carotti, A. Coumarin Derivatives as Dual Inhibitors of Acetylcholinesterase and Monoamine Oxidase. *J. Med. Chem.* **2001**, *44*, 3195–3198.

(21) Novaroli, L.; Reist, M.; Favre, E.; Carotti, A.; Catto, M.; Carrupt, P.-A. Human Recombinant Monoamine Oxidase B as Reliable and Efficient Enzyme Source for Inhibitor Screening. *Bioorg. Med. Chem.* **2005**, *13*, 6212–6127.

(22) Carotti, A.; Altomare, C.; Catto, M.; Gnerre, C.; Summo, L.; De Marco, A.; Rose, S.; Jenner, P.; Testa, B. Lipophilicity Plays a Major Role in Modulating Monoamine Oxidase B (MAO-B) Inhibition by 7-Substituted Coumarins. *Chem. Biodiversity* **2006**, *3*, 134–149.

(23) Catto, M.; Nicolotti, O.; Leonetti, F.; Carotti, A.; Favia, A.; Soto-Otero, R.; Mendez-Alvarez, E.; Carotti, A. Structural Insights into Monoamine Oxidase Inhibitory Potency and Selectivity of 7-Substituted Coumarins from Ligand- and Target-Based Approaches. *J. Med. Chem.* **2006**, *49*, 4912–4925.

(24) Novaroli, L.; Daina, A.; Favre, E.; Bravo, J.; Carotti, A.; Leonetti, F.; Catto, M.; Carrupt, P. A.; Reist, M. Impact of Species-Dependent Differences on Screening, Design, and Development of MAO B Inhibitors *J. Med. Chem.* **2006**, *49*, 6264–6272.

(25) (a) Thompson, L. A.; Ellman, J. A. Synthesis and Applications of Small Molecule Libraries. *Chem. Rev.* **1996**, *96*, 555–600. (b) Nefzi, A.; Ostresh, J. M.; Houghten, R. A. The Current Status of Heterocyclic Combinatorial Libraries. *Chem. Rev.* **1997**, *97*, 449–472. (c) Bunin, B. A.; Dener, J. M.; Livingston, D. A. Application of Combinatorial and Parallel Synthesis to Medicinal Chemistry. *Annu. Rep. Med. Chem.* **1999**, *34*, 267–286. (d) Franzén, R. G. Recent Advances in the Preparation of Heterocycles on Solid Support: A Review of the Literature. *J. Comb. Chem.* **2000**, *2*, 195–214.

(26) Dolle, R. E. Comprehensive Survey of Combinatorial Library Synthesis: 2001. *J. Comb. Chem.* **2002**, *4*, 369–418.

(27) Kate, S. A., Albericio, F., Eds. *Solid-Phase Synthesis: A Practical Guide*; Marcel Dekker: New York, 2000.

(28) Ley, S. V.; Baxendale, I. R.; Bream, R. N.; Jackson, P. S.; Leach, A. G.; Longbottom, D. A.; Nesi, M.; Scott, J. S.; Storer, R. I.; Taylor, S. J. Multi-Step Organic Synthesis Using Solid-Supported Reagents and Scavengers: A New Paradigm in Chemical Library Generation *J. Chem. Soc., Perkin Trans. 1* **2000**, 3815–4195.

(29) Bhattacharyya, S.; Fan, L.; Vo, L.; Labadie, J. Titanium(IV) Isopropoxide Mediated Solution Phase Reductive Amination on an Automated Platform: Application in the Generation of Urea and Amide Libraries. *Comb. Chem. High Throughput Screening* **2000**, *3*, 117–124.

(30) Hughes, D. L. Progress in the Mitsunobu Reaction. *Org. Prep. Proced. Int.* **1996**, *28*, 127–164.

(31) Robinson, D. S.; Lovenberg, W.; Keiser, H. Sjoerdsma Effects of Drugs on Human Blood Platelet and Plasma Amine Oxidase Activity in Vitro and in Vivo. *Biochem. Pharmacol.* **1968**, *17*, 109–119.

(32) Westhead, D. R.; Clark, D. E.; Murray, C. W. A Comparison of Heuristic Search Algorithms for Molecular Docking. *J. Comput.-Aided Mol. Des.* **1997**, *11*, 209–228.

JM070725E